CHEMISTRY
A EUROPEAN JOURNAL

DOI: 10.1002/chem.200902151

Phase-Controlled Synthesis of Transition-Metal Phosphide Nanowires by Ullmann-Type Reactions

Junli Wang,[a] Qing Yang,*[a] Zude Zhang,[a] and Shouheng Sun[b]

Abstract: Transition-metal phosphide nanowires were facilely synthesized by Ullmann-type reactions between transition metals and triphenylphosphine in vacuum-sealed tubes at 350–400 °C. The phase (stoichiometry) of the phosphide products is controllable by tuning the metal/PPh_3 molar ratio and concentration, reaction temperature and time, and heating rate. Six classes of iron, cobalt, and nickel phosphide (Fe_2P, FeP, Co_2P, CoP, Ni_2P, and NiP_2) nanostructures were prepared to demonstrate the general applicability of this new method. The resulting phosphide nanostructures exhibit interesting phase- and composition-dependent magnetic properties, and magnetic measurements suggested that the Co_2P nanowires with anti-$PbCl_2$ structure show a ferromagnetic–paramagnetic transition at 6 K, while the MnP-structured CoP nanowires are paramagnetic with Curie–Weiss behavior. Moreover, GC-MS analyses of organic byproducts of the reaction revealed that thermally generated phenyl radicals promoted the formation of transition-metal phosphides under synthetic conditions. Our work offers a general method for preparing one-dimensional nanoscale transition-metal phosphides that are promising for magnetic and electronic applications.

Keywords: nanostructures · magnetic properties · transition metals · phosphides · C–C coupling

Introduction

Transition-metal phosphides are an important class of functional materials that exhibit a wide range of properties such as magnetism, superconductivity, magnetocaloric effect, magnetoresistance, catalysis, and lithium intercalation.[1–4] However, phase (stoichiometry) control of these phosphides with desired composition is still a huge challenge owing to their complicated stoichiometries (typical formulas: M_4P, M_3P, M_2P, MP, M_2P_3, MP_2, M_2P_5, MP_3) and the associated complex structures.[5,6] In recent years, considerable efforts have been devoted to the synthesis of nanostructured transition-metal phosphides. For instance, Co_2P nanoparticles supported on silica were synthesized by thermal treatment of $[Co_2(CO)_6\{PPh_2CH_2Si(OEt)_3\}]$ and $[Co_4(CO)_{10}(\mu\text{-}[(Ph_2P)_2NH])]$ at high temperatures (500–900 °C).[7] Nanostructured Co_2P, Ni_2P, CoP, FeP, and MnP were prepared by hydrothermal and solvothermal methods using yellow phosphorus (P_4)[8,9] and by a desilylation strategy using tris(trimethylsilyl)phosphine ($P(SiMe_3)_3$).[10] Moreover, Fe_2P, FeP, Co_2P, CoP, Ni_2P, and MnP nanocrystals were also made by solution-phase methods using trioctylphosphine (TOP), metal phosphine complexes, long-chain alkylphosphonic acids, and single-source molecular precursors containing elemental metal and phosphorus.[11–15] Despite these synthetic achievements, the phase or stoichiometry of these nanostructured transition-metal phosphides is not well controlled, except for the phase-tuned synthesis of Fe_2P and FeP nanostructures[13c] reported shortly after submission of this work. More effort is needed to reveal the phase evolution and formation mechanism of transition-metal phosphide nanostructures, and a complete understanding of these processes is of much importance for addressing functional properties and technological potentials of phosphides with specific phases.

Herein we report a new Ullmann-type reaction strategy for phase-controllable synthesis of transition-metal phosphide nanostructures by reactions of transition-metal powders with triphenylphosphine in vacuum-sealed tubes. The Ullmann-type reaction strategy has been employed for the

[a] Dr. J. Wang, Prof. Q. Yang, Z. Zhang
Hefei National Laboratory for Physical Science at Microscale and Department of Chemistry
University of Science and Technology of China (USTC)
Hefei, Anhui 230026 (P. R. China)
Fax: (+86) 0551-3606266
E-mail: qyoung@ustc.edu.cn

[b] Prof. S. Sun
Department of Chemistry, Brown University
Rhode Island 02912 (USA)

Supporting information for this article is available on the WWW under http://dx.doi.org/10.1002/chem.200902151.

synthesis of group III–V semiconductor nanocrystals,[16] and can be extended to the preparation of nanoscale transition-metal phosphides [Eq. (1)]

$$PPh_3 + M \rightarrow M_xP_y + Ph{-}Ph \quad (1)$$

where M = Fe, Co, Ni; M_xP_y = Fe_2P, FeP, Co_2P, CoP, Ni_2P, and NiP_2. By using this strategy, phase control in M_xP_y nanostructures was readily achieved by rationally controlling preparation parameters, such as precursor ratio and concentration, reaction temperature and time, and heating rate. The effects of these parameters on the phase (stoichiometry) of the phosphide products were intensively studied, and the nature of the crystal growth of the as-synthesized phosphides was examined. GC-MS studies on the organic by-products produced in the reaction revealed that formation of transition-metal phosphides occurred by an Ullmann-type reaction, and a reaction mechanism involving phenyl radicals was suggested, through which six classes of phosphide nanowires of iron, cobalt, and nickel were selectively synthesized. Magnetic measurements showed that the phosphide products display interesting phase- and composition-dependent magnetic properties. The current route provides a new and general chemical method for tunable preparation of transition-metal phosphide nanostructures, which are significant for further magnetic and electronic studies.

Results and Discussion

Selective synthesis of Co_2P and CoP nanowires exemplifies the phase control achieved by our method. The synthetic details are described in the Experimental Section, and the synthetic conditions are summarized in Table 1, which shows that phase control of Co_2P and CoP nanostructures is successfully realized by adjusting the feedstock (Co and PPh_3) ratio and concentration, reaction temperature and time, and heating rate.

Table 1. Summary of preparation conditions for the phase control of Co_2P and CoP nanowires.

Entry	Co/P molar ratio [mmol/mmol]	Heating time[a] [min]	*T*/*t* [°C/h]	Products
1	4:1	200	370–385/15	Co_2P
2	2:1	200	370–385/15	Co_2P
3	1:2	200	370/15	Co_2P
4	1:2	60	370/15	Co_2P+CoP
5	1:2	60	370/15	Co_2P[b]
6	1:2	200	385/8	Co_2P+CoP
7	1:2	200	385/15	CoP
8	2:4	200	385/15	Co_2P+CoP
9	1:4	60	385/15	CoP
10	1:4	200	385/15	CoP
11	1:4	200	385/8	CoP
12	1:4	200	385/4	Co_2P+CoP
13	1:4	200	370/15	CoP
14	1:4	200	370/8	Co_2P+CoP
15	1:4	200	370/15	Co_2P[b]
16	1:4	200	355/15	Co_2P+CoP
17	1:4	200	355/24	Co_2P+CoP
18	1:6	200	370–385/15	CoP

[a] From room temperature to the designated temperature. [b] With addition of 4 mmol biphenyl.

Powder X-ray diffraction (XRD) was used to characterize the crystal structure and phase purity of the products. Figure 1 shows XRD patterns for Co_2P and CoP samples obtained in the typical syntheses (see Experimental Section). The diffraction peaks of the Co_2P and CoP samples match well with the reference patterns for Co_2P (JCPDS No. 89-3030) and CoP (JCPDS No. 89-4862), and can be assigned to the orthorhombic anti-$PbCl_2$ structure and the orthorhombic MnP structure,[5,6] respectively. No other peaks from impurities are detected in these XRD patterns, that is, the as-synthesized crystalline phosphide products are phase-pure within the limit of detection of the XRD technique employed.

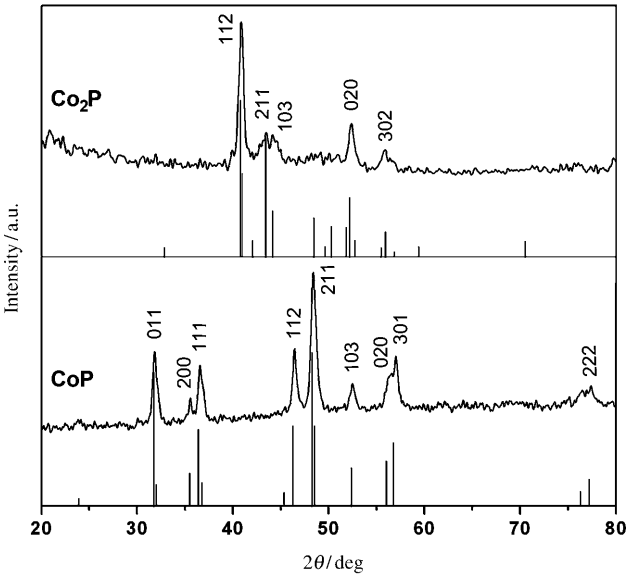

Figure 1. XRD patterns of Co_2P and CoP nanowire samples, with reference patterns of the standard JCPDS cards for Co_2P and CoP.

The morphologies of the as-obtained Co_2P and CoP samples were examined by transmission electronic microscopy (TEM). Figure 2 displays TEM images for samples obtained under different preparative conditions. The samples generally have a wirelike shape, and the aspect ratio of these wires can be tuned by changing the Co/PPh_3 molar ratio. Figure 2a and b show long Co_2P nanowires with diameters of 10–20 nm and lengths of up to several micrometers obtained at high Co/PPh_3 ratios, and Figure 2c and d relatively short nanowires or nanorods of Co_2P and CoP obtained at low Co/PPh_3 ratios. Overall, the Co_2P nanowires have a higher aspect ratio than the CoP nanowires (see Figure 2 and Figure S1 in the Supporting Information).

As demonstrated in Table 1, the synthetic conditions have considerable influence on the morphology and structure of Co_2P and CoP nanowires. The precursor molar ratio and

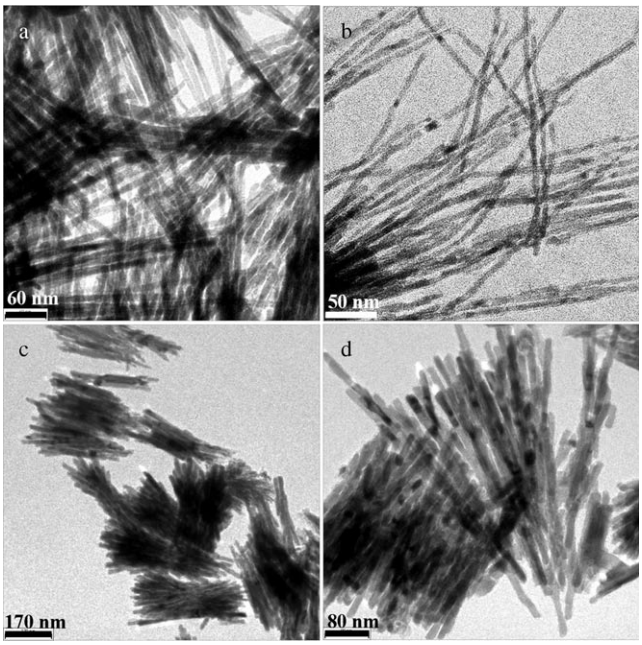

Figure 2. TEM images of a), b) and c) Co_2P nanowires obtained at Co/PPh_3 molar ratios of 4:1 (a), 2:1 (b), and 1:2 (c), corresponding to entries 1, 2, and 3 in Table 1; and d) CoP nanowires obtained at a Co/PPh_3 molar ratio of 1:4 (entry 10 in Table 1).

concentration strongly affect the product phase (stoichiometry). In general, high PPh_3 concentration (ratio) favors the production of pure CoP nanowires of high P content. Conversely, Co_2P nanowires are obtained. With Co/PPh_3 molar ratios ranging from 4:1 to 1:2, pure Co_2P nanowires/nanorods can be synthesized, while pure CoP nanorods are produced at lower Co/PPh_3 molar ratios of 1:4 to 1:6. To some extent, the heating rate, that is, the heating time in which the reaction temperature rises from room temperature to the designated temperature, can affect the phase purity of the phosphide products. For instance, at a Co/PPh_3 molar ratio of 1:2, a fast heating rate over 60 min yields a mixture of CoP and Co_2P, whereas pure Co_2P is produced at a slow heating rate of 200 min and keeping other synthetic parameters constant (Table 1, entries 3 and 4). This shows that the fast heating rate is helpful to yield high-P CoP. However, with a large excess of PPh_3 (P-rich conditions) with Co/PPh_3 molar ratios of 1:4–6, the change in heating rate does not affect the phase of the final products, and pure CoP nanowires/nanorods are always obtained (Table 1, entries 9, 10, and 18). When the concentration of Co and PPh_3 was doubled without changing the Co/P molar ratio (1:2) or other preparation conditions, a mixture of Co_2P and CoP was obtained (entry 8 in Table 1). We also found that pure Co_2P nanowires could be prepared when 4 mmol of biphenyl was added to 1:2 or even 1:4 Co/PPh_3 mixtures (Table 1, entries 5 and 15). The effects of biphenyl addition on the reactions of Equation (1) and on the phase control of phosphides will be discussed below.

The effects of reaction temperature and time on the phase of Co_2P and CoP nanowires/nanorods were further investigated carefully (Table 1). Relatively high temperature and long time favor the yield of high-P CoP, and low temperature and short time low-P (Co-rich) Co_2P, as confirmed by XRD measurements (see Figure S2 in the Supporting Information). Increasing the temperature effectively restrains formation of Co_2P and tends to yield pure CoP (Table 1, entries 3, 7, 10, 13, and 16). Time-dependent experiments show that a short reaction time leads to the production of a Co_2P/CoP mixture at a Co/PPh_3 molar ratio of 1:2 or 1:4, but as the time increases pure CoP products can be obtained with the disappearance of the Co_2P phase (Table 1, entries 6, 7, 10–17). These results suggest that Co_2P is not a thermodynamically stable phase, just a metastable one, whereas CoP is a relatively stable phase that can be formed by reaction of initially formed Co_2P with PPh_3, besides direct conversion of elemental Co to CoP. The conversion of Co_2P to CoP is also consistent with the trend in the binary Co–P phase diagram (see Figure S3 in the Supporting Information),[5c,d] which shows that Co_2P in either bulk or nanoscale form can be converted to CoP under P-rich conditions, but in general Co_2P could controllably be synthesized by a kinetic process under conditions of relatively lower temperature, shorter reaction time, and lower concentration of PPh_3 (Table 1, entries 1–3, 6, 7, 12, 14–17).

The reactions of Equation (1) indicate that both Co_2P and CoP are obtained by conversion of elemental Co to phosphide in PPh_3 medium. The molar ratio and concentration of Co and P atoms in this conversion process are considered to play important roles in the phase control of Co_2P to CoP nanowires/nanorods in the thermodynamic growth regime. The phases of cobalt phosphides are closely dependent on preparation parameters and can be controlled by variation of these parameters. Increasing PPh_3 fraction (concentration), reaction temperature and time, and heating rate improve the conversion, and under such conditions the reaction and incorporation of phosphorus with metal atoms are greatly promoted. Similar cases have also been documented previously.[13c,14a] Consequently, the production of high-P content CoP is realized. Interestingly, addition of biphenyl to the reaction favors the formation of low-P (metal-rich) Co_2P. On one hand, the addition of biphenyl lowers the concentrations of Co and PPh_3 and suppresses the interaction between Co and P. On the other hand, as one of products of reaction, addition of biphenyl will suppress the reactions of Equation (1) towards the right-hand side in a fast rate kinetically and can alter the equilibrium of the reaction thermodynamically. Accordingly, the Co_2P of lower P content is produced.

The structure of Co_2P and CoP nanowires was further characterized by high-resolution TEM (HRTEM) and electron diffraction (ED). The TEM, HRTEM, and ED images for Co_2P and CoP nanowires are shown in Figure 3. Figure 3a is a typical TEM image of Co_2P nanowires, and the matching HRTEM image and ED pattern are shown in Figure 3b. In the Co_2P structure, the crystal grows perpendicular to the (020) planes, that is, in the [020] (i.e., [010]) direction for an orthorhombic structure. Figure 3c and d show

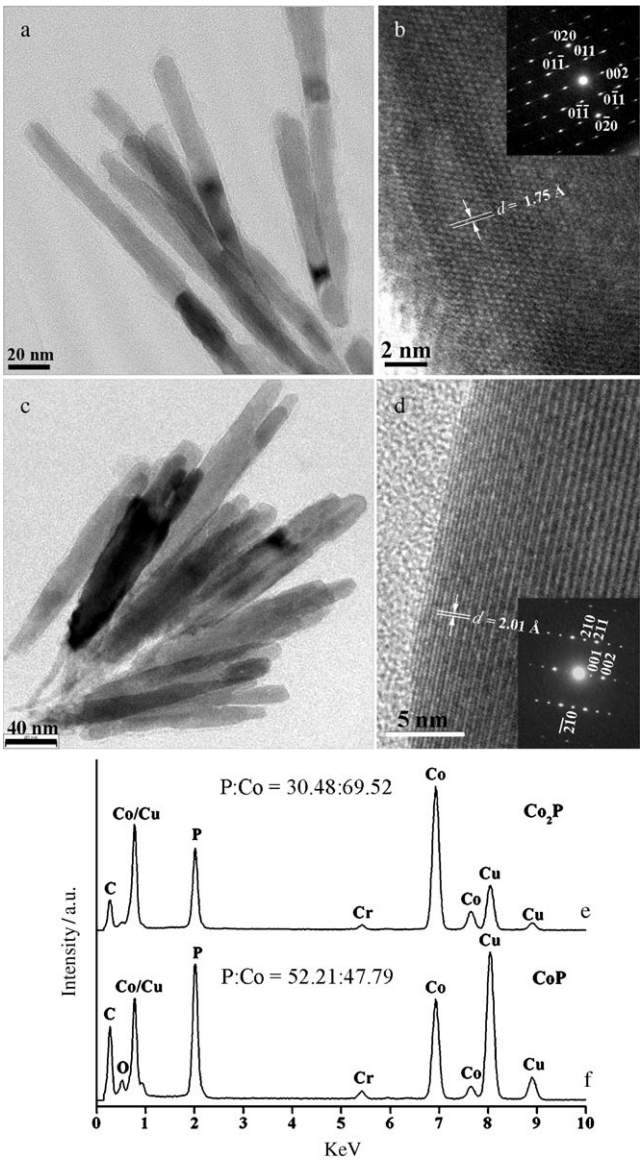

Figure 3. TEM and HRTEM images and SAED patterns (insets) of a), b) Co_2P nanowires; c), d) CoP nanowires. e), f) EDX spectra of the Co_2P and CoP nanowires.

TEM and HRTEM images and the ED pattern of CoP nanowires. The as-synthesized CoP nanowires have the preferred growth direction perpendicular to the (210) planes or parallel to the (002) planes. The preferred growth direction of Co_2P nanowires agrees with the case reported in the literature,[12b] whereas that of CoP nanowires is different from the prior report, wherein CoP nanowires prefer to grow on parallel to the (011) planes.[15a] For an orthorhombic crystal structure, anisotropic growth usually takes place preferentially in the [010] direction because of the higher surface energy of the (010) planes compared to other planes.[14d] Accordingly, the obtained Co_2P nanowires/rods grown in the [010] direction are longer than CoP nanowires/nanorods (Figure 2 and Figure S1 in the Supporting Information). The conversion from Co_2P to CoP via the successive reaction of preformed Co_2P with PPh_3, which occurs in the growth of CoP nanorods, can cause the breakdown of long Co_2P nanowires and leads to relatively short CoP nanorods. Similarly, Brock et al. also found that long Fe_2P nanorods could be converted to small FeP nanoparticles in phase-controlled synthesis.[13c] Moreover, these HRTEM and ED studies reveal the good crystallinity of both Co_2P and CoP nanowires, consistent with what is concluded from the XRD studies. The chemical compositions of Co_2P and CoP were further characterized by energy dispersive X-ray (EDX) spectroscopy (Figure 3e and f). The results correspond to the Co_2P and CoP formulae, although there is a slight difference between the detected Co/P ratios and those of stoichiometric Co_2P and CoP (2:1 and 1:1). The discrepancy can be explained in terms of the limitations of the EDX technique (which is semiquantitative) and the possibility of impurity phases in the products.

The surface chemical nature of Co and P in the Co_2P and CoP samples was characterized by X-ray photoelectron spectroscopy (XPS, Figure 4). The XPS spectra (Figure 4a) indicate the presence of Co and P along with C from the reference and O from absorbed and oxidized species. The Co $2p_{3/2}$ binding energies for the Co_2P and CoP products are centered at 778.49 and 779.02 eV, respectively, in good agreement with reported data.[17] Figure 4b and c show high-resolution XPS spectra of the P 2p region. In the close-up P 2p spectrum of Co_2P (Figure 4b), the broad peak centered at 133.47 eV on the high binding-energy side is assigned to the P 2p signal from oxidized P species, and the peaks at 130.59 and 129.73 eV agree well with P $2p_{1/2}$ and P $2p_{3/2}$ from Co_2P. Similarly, the high-resolution P 2p region for CoP (Figure 4c) also shows two peaks, at 130.67 and 129.75 eV, that reflect the binding energy of P $2p_{1/2}$ and P $2p_{3/2}$. The results are consistent with the previous observations that the P 2p region of transition-metal phosphides usually splits into two peaks for P $2p_{1/2}$ and P $2p_{3/2}$ in high-resolution XPS spectra.[17] The peak centered at 133.93 eV corresponds to P 2p from oxidized P. The presence of oxidized P species in the samples is probably due to two processes: separation of product in air after the reaction, which can lead to surface oxidization of nanoscale phosphides due to absorbed gaseous molecules indicated by the close-up oxygen XPS spectrum, which are often observed in nanomaterials,[16b] and oxidization of phosphides by residual oxygen in the sealed tube during reaction.

Magnetic properties of the Co_2P and CoP nanowires were measured on a SQUID magnetometer (Quantum Design, MPMS). Figure 5 shows the temperature dependence of magnetization (M–T) for the Co_2P and CoP nanowires. Zero-field cooling (ZFC, filled circles) and field cooling (FC, open circles) curves show that Co_2P and CoP nanowires exhibit different magnetic properties. As shown in Figure 5a, the FC M–T curve for the Co_2P nanowires rises monotonically with decreasing temperature, and the ZFC curve exhibits a transformation temperature at 6 K, above which the curve declines monotonically to a plateau as the temperature rises. The transformation temperature at 6 K is consid-

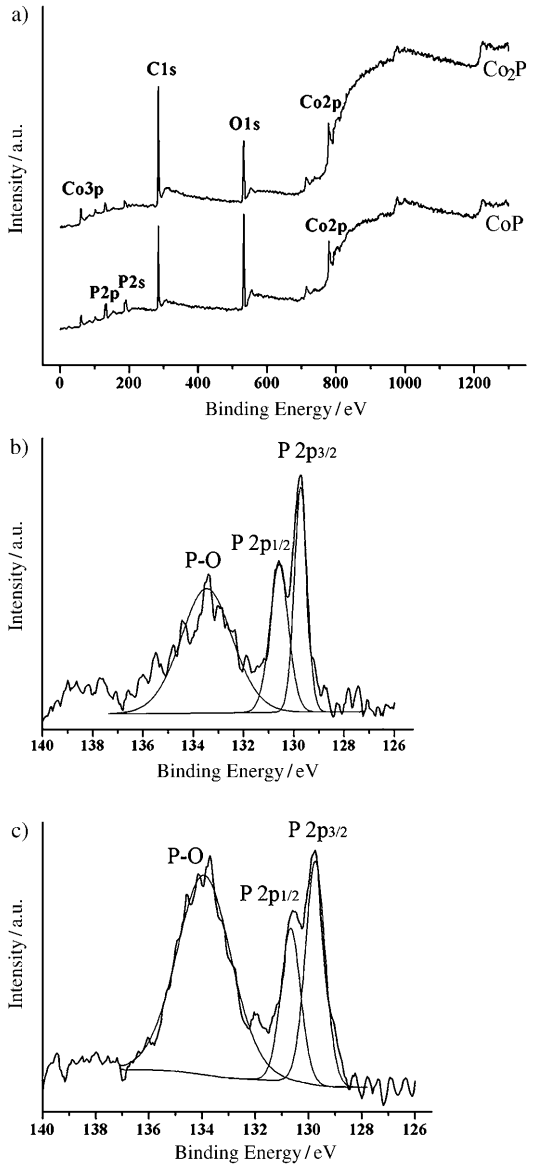

Figure 4. XPS spectra. a) Survey spectra, b) and c) high-resolution spectra of P 2p region for the Co_2P and CoP nanowires.

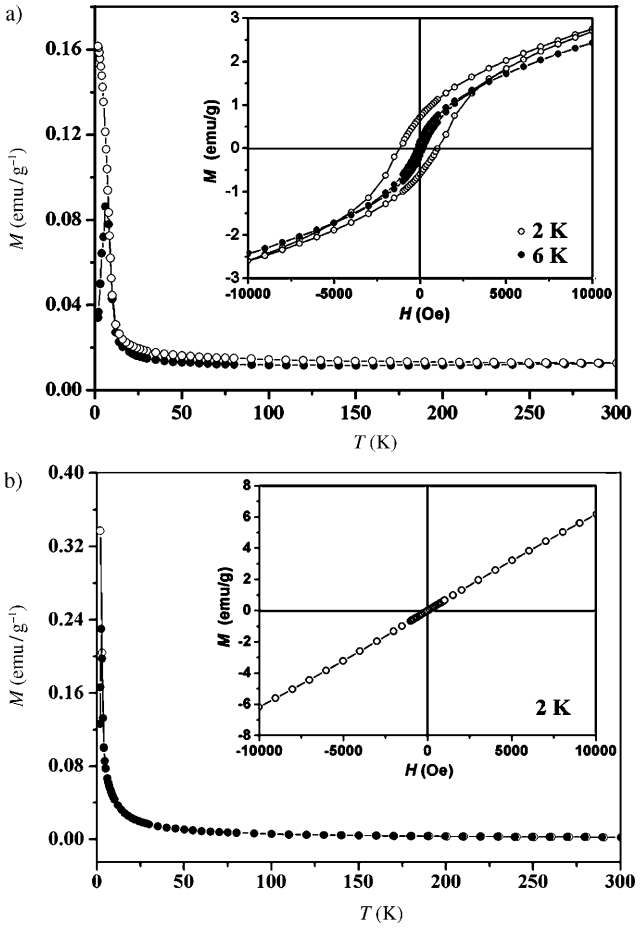

Figure 5. Temperature dependence of magnetization for samples of a) Co_2P and b) CoP nanowires prepared by typical syntheses. The insets display the field dependence of the magnetization at 6 and 2 K.

ered to be the Curie temperature T_C, at which Co_2P nanowires change from paramagnetic to ferromagnetic. The change of magnetic properties for Co_2P nanowires is confirmed by the presence of magnetization hysteresis loops at 6 and 2 K (inset of Figure 5a), and the loops have coercivities of about 160 and 1100 Oe, respectively. The above magnetic behavior of the Co_2P nanowires is different from those reported in previous studies, in which bulk Co_2P is Pauli paramagnetic[3a,12b] and nanostructured Co_2P follows the Curie–Weiss law but without a Curie temperature.[8b,12b] The ferromagnetic–paramagnetic transition may be ascribed to trace elemental Co impurity embedded inside Co_2P nanowires/nanorods. However, such trace Co impurity can not be detected by XRD within its detection limit (ca. 2%) and could not be washed off from the sample with dilute HCl in the experiments due to the diffusion-limited process resulting from the protection of Co by Co_2P; many metal phosphides, for example, those of Co, Fe, Ni, and In, are markedly resistant to etching by dilute HCl.[5a,16] A nanocomposite containing cobalt nanoparticles was reported to display similar magnetic properties to our Co_2P nanorods.[18] For comparison, magnetic measurements showed that CoP nanowires are paramagnetic and have Curie–Weiss behavior (Figure 5b).

The synthesis of Co_2P and CoP nanowires can be extended to other types of transition-metal phosphide nanostructures. Using this method, we have also prepared pure Fe_2P, FeP, Ni_2P, and NiP_2 nanostructures. The phase control of nanoscale iron and nickel phosphides is also realized by rationally controlling the preparation conditions, as described in the Experimental Section. The phase and purity of the resulting products were checked by XRD (shown in Figure 6). All of the diffraction peaks in the XRD patterns can be assigned to pure hexagonal Fe_2P (JCPDS No. 88-1803), orthorhombic FeP (JCPDS No. 89-2746), hexagonal Ni_2P (JCPDS No. 89-4864), and cubic NiP_2 (JCPDS No. 73-0436), respectively.

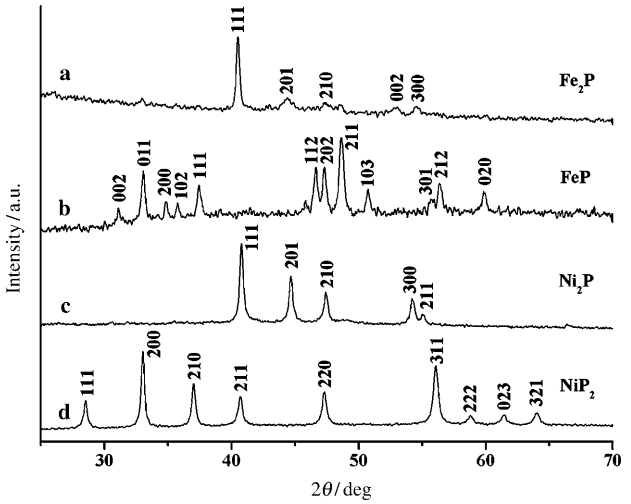

Figure 6. XRD patterns of transition-metal phosphide nanowires. a) Fe_2P, b) FeP, c) Ni_2P, and d) NiP_2.

Figure 7 displays TEM images of the Fe_2P, FeP, Ni_2P, and NiP_2 nanostructures. The TEM investigations (Figure 7a, b) reveal that Fe_2P and FeP have high aspect ratio with an average diameter of 15 nm and lengths of micrometers. Ni_2P has the same structure as Fe_2P but shows a branched nanowire structure (Figure 7c). The NiP_2 products have a rodlike shape (Figure 7d).

High-resolution TEM and ED studies (Figure 8 and Figure S4 in the Supporting Information) were performed to characterize the quality and microstructure of the as-synthesized iron and nickel phosphide nanostructures. The HRTEM images and ED patterns indicate that the Fe_2P nanowires grow in the [001] direction (Figure 8a and Figure S4a), FeP nanowires parallel to the (200) plane, that is, perpendicular to the (013) planes (Figure 8b and Figure S4b in the Supporting Information), and branched Ni_2P nanostructures parallel to the (110) plane (Figure 8c and Figure S4c in the Supporting Information). The preferential growth directions of the Fe_2P and FeP nanowires are consistent with earlier studies,[11b,12] whereas that of branched Ni_2P nanowires is different.[12b] Furthermore, the ED pattern and HRTEM image of cubic NiP_2 rodlike nanocrystals, shown in Figure 8d and Figure S4d in the Supporting Information, can be indexed to the diffraction spots and lattice planes of the cubic NiP_2 [001] zone.

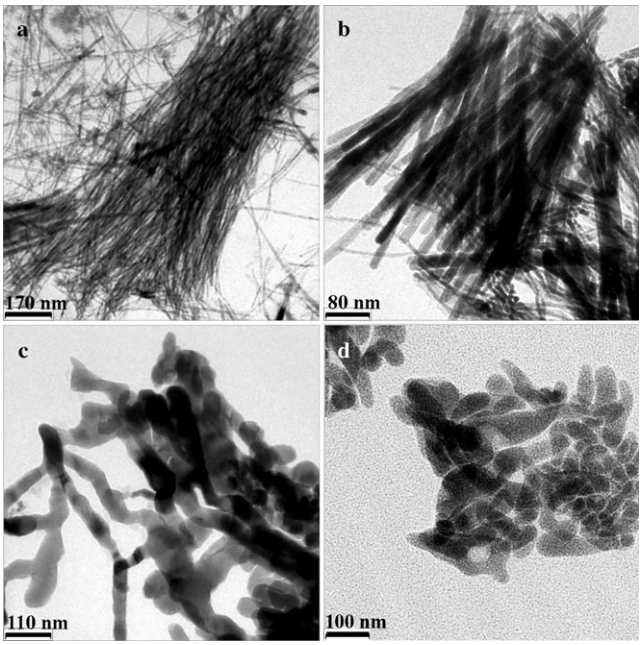

Figure 7. TEM images of a) Fe_2P nanowires, b) FeP nanowires, c) branched Ni_2P nanostructures, and d) rodlike NiP_2.

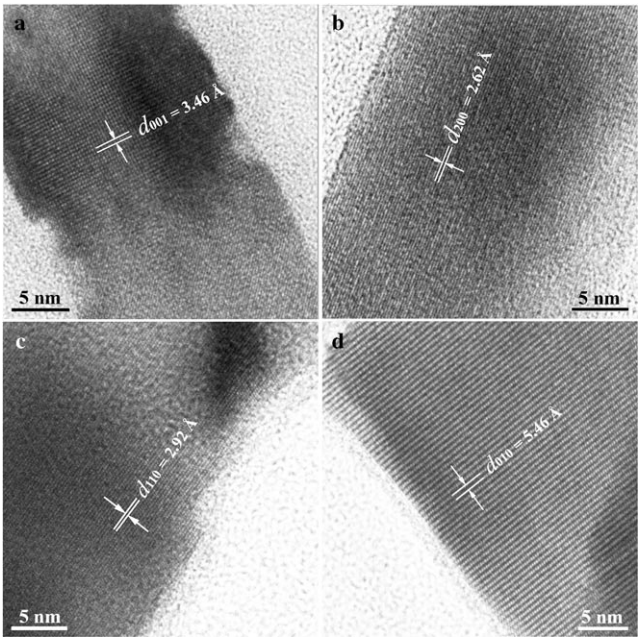

Figure 8. HRTEM images and ED patterns taken on the samples of a) Fe_2P nanowires, b) FeP nanowires, c) branched Ni_2P nanostructures, and d) rodlike Ni_2P.

Brock and co-workers recently demonstrated controlled synthesis of Fe_2P and FeP nanoparticles via a solution-based route (after submission of current work), wherein TOP was used as the phosphorus precursor.[13c] In our work, PPh_3 plays a key role in the phase control of nanoscale transition-metal phosphides. From the aspect of the temperature difference in the synthesis of metal phosphide nanocrystals, it can be simply considered that the P–C bond of PPh_3 (350–400 °C)[16] is stronger than the P–Si bond of $P(SiMe_3)_3$ (220–320 °C)[10,19] and the P–C bond of TOP (300–380 °C).[11–14] Among the three precursors, PPh_3 has relatively high P–C bond strength and is more stable, which could make cleavage of the P–C bond more difficult, but is helpful in controlling the rate of P–C bond cleavage. In the region of activation temperatures (350–400 °C), limited by the strong P–C bonds of PPh_3, the reaction and incorporation of phosphorus with metal atoms are not too fast to be controlled. At a slow rate of reaction and incorporation, low-P content Co_2P is produced, while high-P content CoP is formed at a fast

rate, which can be achieved by increasing reaction temperature and PPh_3 concentration and heating rate. As a consequence, the phase control of transition-metal phosphide nanostructures is achieved.

Extraction of phosphorus from PPh_3 to synthesize metal phosphide nanostructures is a phenyl elimination and coupling process.[16] This is a new variant of the classical Ullmann reaction.[20] To further understand the mechanism of reaction (1) at the molecular level, we examined the organic byproducts formed in the synthetic reaction between transition metals (Co, Fe, and Ni) and PPh_3 by GC-MS. The results of GC-MS analyses for the organic byproducts produced in the reaction of Co and PPh_3 in a 4:1 molar ratio are shown in Table 2 and Figure S5 in the Supporting Information. Biphenyl, three terphenyl isomers, and tetraphenyl isomers dominate the organic byproducts, among which biphenyl is the main byproduct. This reveals phenyl coupling occurred under reaction conditions, typically in vacuum-sealed tubes at 350–400 °C, that are kinetically favorable for thermal generation of phenyl radicals. A phenyl radical reaction mechanism for our new Ullmann-type reaction is concisely illustrated in Scheme 1, by which the formation of CoP and organic byproducts such as biphenyl, terphenyl and tetraphenyl can be rationally explained. Previous work showed that photolysis can decompose PPh_3 in benzene solution to give diphenylphosphinyl radicals ($PPh_2^{\bullet}$) and phenyl radicals ($Ph^{\bullet}$), which rapidly combine to form Ph_2P-PPh_2 and Ph–Ph.[6] In the current work, PPh_3 decomposition to produce active $PPh_2^{\bullet}$ and $Ph^{\bullet}$ radicals is induced by thermolysis and metal catalysis at elevated temperatures (350–400 °C). Subsequently, $Ph^{\bullet}$ radicals will collide with each other and immediately combine to form biphenyl (Ph–Ph), an organic species stable at elevated temperatures.[21] Therefore, biphenyl is the main component of the organic byproducts, as established by the GC-MS analysis. Because biphenyl is one of the main reaction products, addition of biphenyl to the reactants (Co and PPh_3) will significantly alter the equilibrium of reactions (1) and displace them towards the left-hand side. Accordingly, the phosphide phase is changed by addition of biphenyl, and the reactions tend to yield low-P or metal-rich phases (e.g., Co_2P), as is confirmed in entries 5 and 15 of Table 1. Thus, the experiments with biphenyl addition also support the proposed mechanism, besides the GC-MS studies. The $PPh_2^{\bullet}$ radicals are unable to combine to form Ph_2P-PPh_2 at temperatures of 350–400 °C. The $PPh_2^{\bullet}$ radicals are more reactive and will bind to Co atoms to form stable Co–P bonds. We assume that $M-PPh_2$ complexes could exist as intermediates containing Co–P bond, but are stable at high temperature, continue to release $Ph^{\bullet}$ radicals under Co catalysis, and finally yield pure CoP.

Table 2. Organic by-products determined by GC-MS.

Sample no.	Components [%]		
	Biphenyl	terphenyls	tetraphenyls and other by-products
1	65.00	(7.49+11.22+7.66)	8.63
2	64.57	(3.25+12.31+8.20)	9.06
3	65.94	(4.56+11.73+8.00)	9.77

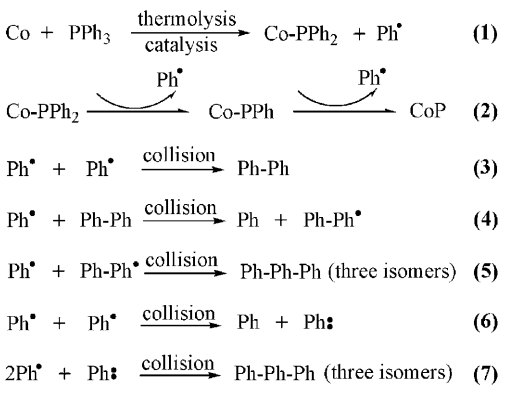

Scheme 1. Proposed reaction mechanism of phenyl radicals in the Ullmann-type reaction between Co and PPh_3.

Under the current reaction conditions, $Ph^{\bullet}$ radicals can collide with PhPh to generate $PhPh^{\bullet}$ and PhH (benzene), and combination of $PhPh^{\bullet}$ with $Ph^{\bullet}$ leads to the formation of terphenyls. $PhPh^{\bullet}$ has three kinds of chemical structure, and accordingly three terphenyl isomers are present in the organic products. The increased of benzene content in the organic byproducts is seen in the GC-MS measurement (Figure S6 in the Supporting Information), which is further support for the proposed reaction mechanism. Alternatively, $Ph^{\bullet}$ radicals can self-collide to generate PhH and phenyl biradicals (Ph:).[22] One Ph: biradical combines with two $Ph^{\bullet}$ radicals to produce terphenyls, and three kinds of Ph: structures generate the three corresponding terphenyl isomers. It is believed that tetraphenyls are produced in a similar way to the above two possible routes.

Furthermore, the current synthetic system is favorable for reactions of thermally generated phenyl radicals at elevated temperature, which promote formation of transition-metal phosphides. Radical reactions frequently occur in vapor/gas phase, and are often induced by photolysis, thermolysis, and catalysis.[23] In our synthesis, the employed temperature (350–400 °C) is higher than or comparable to the boiling points of triphenylphosphine (377 °C), benzene (80.1 °C), biphenyl (254 °C), and terphenyl (383 °C), and creates a vapor-phase environment for the reaction in vacuum-sealed tubes. The vapor-phase environment provides a good platform for reaction of the phenyl radicals. Meanwhile, thermolysis and metal catalysis also favor the production, collision, and propagation of phenyl radicals in the present synthesis. Thereby, the phenyl radical mechanism we propose is reasonable, although the phenyl radical has not been detected by ESR due to the short-lived highly reactive nature of radicals at high temperatures. This mechanism can be also applicable to the reactions of other metals with PPh_3 in the synthesis of transition or main-group metal phosphides, including Co_2P, Fe_2P, FeP, Ni_2P, NiP_2, and InP.

Conclusion

We have demonstrated a general method for the phase (stoichiometry) controlled synthesis of transition-metal phosphide nanowires. The synthesis relies on a new Ullmann-like reaction of elemental metals with PPh_3 in vacuum-sealed tubes. Phase control is achieved by carefully controlling preparation parameters, including metal/PPh_3 ratio and concentration, reaction temperature and time, and heating rate. Six types of cobalt, iron, and nickel phosphide nanowires were synthesized. These high quality nanowires display distinct structural characteristics and magnetic properties. Based on GC-MS studies on organic byproducts, it is concluded that the phosphides are formed through an Ullmann-type reaction of phenyl radicals. The present work provides a new strategy for the selective synthesis of transition-metal phosphide nanostructures for potential magnetic and electronic applications.

Experimental Section

Phase-controlled synthesis of Co_2P and CoP nanowires: In a typical synthesis of Co_2P nanowires, a mixture of Co powder (0.118 g, 2 mmol, AR, >99.5%) and PPh_3 (0.265 g, 1 mmol, CP, 99%) was put into a quartz ampullaceous tube (∅ 1 cm×15 cm), which was then evacuated and sealed. The sealed tube was loaded into a resistance furnace by a tilt angle of 5°, heated from room temperature to 385 °C over 200 min, and kept at this temperature for 15 h. After the tube was allowed to cool to room temperature, the black products were collected, washed with benzene, dilute hydrochloric acid, and absolute ethanol, and finally dried in a vacuum furnace at 60 °C for further investigation. The Co_2P sample was washed in dilute hydrochloric acid (ca. 1–2 M) in an oven at 60–70 °C for several hours to removed unconverted Co particles, especially for the syntheses with excess Co (Co/PPh_3 > 1:1). Without changing other synthetic conditions, CoP nanowires were also obtained by increasing the molar ratio of Co/PPh_3 to 1:4. No HCl treatment was needed for the CoP nanowire sample. The details of the phase-controlled synthesis are summarized in Table 1.

Selective synthesis of Fe_2P, FeP, Ni_2P, and NiP nanostructures: Fe powder or Ni powder was first treated with 0.1 m $NaBH_4$ aqueous solution by sonication to remove surface oxides. 1.000 g of Fe powder or Ni powder was mixed with 10 mL of $NaBH_4$ aqueous solution and sonicated for 10 min. The metal powder was separated by decanting the upper solution layer and washed with distilled water and anhydrous ethanol three times each, and finally dried in a vacuum furnace at 50 °C for further use. In the synthesis of Fe_2P and Ni_2P nanowires, a mixture of the $NaBH_4$-treated Fe or Ni powder and PPh_3 with a molar ratio of 4:1 or 2:1.2 was put into a quartz ampullaceous tube (∅ 1 cm×15 cm). The tube was then evacuated and sealed. The sealed tube was loaded into a resistance furnace by a tilt angle of 5°, heated from room temperature to 380 °C in 100 min, and kept at this temperature for 15 h. The following procedures were identical to those used for Co_2P synthesis. In addition, FeP and NiP_2 were prepared similarly, except that the ratios of Fe/PPh_3 and Ni/PPh_3 were kept at 1:4 with a heating rate of 60 min from room temperature to 390 °C.

Characterization: The crystal structure and phase purity of the transition-metal phosphide nanowires were examined by powder X-ray diffraction (XRD, Philips X'Pert Pro Super diffractometer) with graphite-monochromatized $Cu_{K\alpha}$ radiation (λ = 1.54178 Å). Electron diffraction (ED), energy dispersive X-ray spectrometry (EDX), low- and high-resolution transmission electronic microscopy (HRTEM) data were collected on a JEOL JEM-2011 electron microscope operating at 200 kV. Samples for TEM analysis were prepared by sonicating the products in ethanol and dropping a small volume onto a carbon-coated copper grid. X-ray photoelectron spectroscopy (XPS) measurements were performed on a VGESCA-LAB MKII X-ray photoelectron spectrometer with an $Al_{K\alpha}$ excitation source. The magnetic properties of Co_2P and CoP nanorods were measured with a Quantum Design MPMS-XL7 SQUID magnetometer, and the temperature dependence of magnetization was measured in an applied magnetic field of 100 Oe between 2 and 300 K by using zero-field cooling (ZFC) and field-cooling (FC) procedures. The organic byproducts produced from the synthesis were tested on a Thermo Finnigan gas chromatograph with a Varian 8cb 30 m×0.25 mm×0.25 μm column, coupled with a mass spectroscopic detector (GC-MS).

Acknowledgements

Financial support from the K. C. Wong Education Foundation of Hong Kong, the National Nature Science Foundation of China (Grants 20571068), the Program for New Century Excellent Talents at the university from Chinese Ministry of Education (NCET2006-0552), Anhui Provincial Education Department (No. KJ2008A071), Creative Research Foundation for Graduate of USTC (No. KD2008019), and the CAS Special Grant for Postgraduate Research, Innovation and Practice (2008) is gratefully acknowledged.

[1] a) S. Ohta, H. Onmayashiki, *Physica B: Condens. Matter* **1998**, *253*, 193; b) F. Gillot, S. Boyanov, L. Dupont, M. L. Doublet, M. Morcrette, L. Monconduit, J. M. Tarascon, *Chem. Mater.* **2005**, *17*, 6327.
[2] O. Tegus, E. Brück, K. H. J. Buschow, F. R. de Boer, *Nature* **2002**, *415*, 150.
[3] a) S. Fujii, S. Ishida, S. Asano, *J. Phys. F* **1988**, *18*, 971; b) S. T. Oyama, *J. Catal.* **2003**, *216*, 343; c) J. Jiang, S. M. Kauzlarich, *Chem. Mater.* **2006**, *18*, 435; d) D. C. S. Souza, V. Pralong, A. J. Jacobson, L. F. Nazar, *Science* **2002**, *296*, 2012.
[4] M. P. Bichat, J. L. Pascal, F. Gillot, F. Favier, *Chem. Mater.* **2005**, *17*, 6761.
[5] a) B. Arinsson, T. Landstrom, S. Rundquist, *Borides, Silicides and Phosphides*, Wiley, New York, **1965**; b) N. N. Greenwood, A. E. Earnshaw, *Chemistry of the Elements*, Pergamon Press, New York, **1997**; c) M. E. Schlesinger, *Chem. Rev.* **2002**, *102*, 4267; d) *Binary Alloy Phase Diagrams* (Eds.: T. B. Massalski, H. Okamoto, P. R. Subramaniam, L. Kacprzak), 2nd ed., ASM International: Materials Park, OH, **1990**.
[6] D. E. C. Corbridge, *Phosphorus: An Outline of its Chemistry, Biochemistry and Technology*, 3th ed., Elsevier, New York, **1985**.
[7] a) C. M. Lukehart, Stephen B. Milne, S. R. Stock, *Chem. Mater.* **1998**, *10*, 903; b) F. Schweyer-Tihay, P. Braunstein, C. Estournes, J. L. Guille, B. Lebeau, J. L. Paillaud, M. Richard-Plouet, J. Rosé, *Chem. Mater.* **2003**, *15*, 57.
[8] a) Y. Xie, H. L. Su, X. F. Qian, X. M. Liu, Y. T. Qian, *J. Solid State Chem.* **2000**, *149*, 88; b) H. W. Hou, Q. Yang, C. R. Tan, G. B. Ji, B. X. Gu, Y. Xie, *Chem. Lett.* **2004**, *33*, 1272; c) F. Luo, H. L. Su, W. Song, Z. M. Wang, Z. G. Yan, C. H. Yan, *J. Mater. Chem.* **2004**, *14*, 111.
[9] B. M. Barry, E. G. Gillan, *Chem. Mater.* **2008**, *20*, 2618.
[10] a) S. C. Perera, P. S. Fodor, G. M. Tsoi, L. E. Wenger, S. L. Brock, *Chem. Mater.* **2003**, *15*, 4034; b) S. C. Perera, G. Tsoi, L. E. Wenger, S. L. Brock, *J. Am. Chem. Soc.* **2003**, *125*, 13960; c) S. L. Brock, S. C. Perera, K. L. Stamm, *Chem. Eur. J.* **2004**, *10*, 3364.
[11] a) J. H. Chen, M. F. Taib, K. M. Chi, *J. Mater. Chem.* **2004**, *14*, 296; b) C. Qian, F. Kim, L. Ma, F. Tsui, P. D. Yang, J. Liu, *J. Am. Chem. Soc.* **2004**, *126*, 1195.
[12] a) J. Park, B. Koo, Y. Hwang, C. Bae, K. An, J. G. Park, H. M. Park, T. Hyeon, *Angew. Chem.* **2004**, *116*, 2332; *Angew. Chem. Int. Ed.* **2004**, *43*, 2282; b) J. Park, B. Koo, K. Y. Yoon, Y. Hwang, M. Kang, J. G. Park, T. Hyeon, *J. Am. Chem. Soc.* **2005**, *127*, 8433.

[13] a) R. K. Chiang, R. T. Chiang, *Inorg. Chem.* **2007**, *46*, 369; b) K. A. Gregg, S. C. Perera, G. Lawes, S. Shinozaki, S. L. Brock, *Chem. Mater.* **2006**, *18*, 879; c) E. Muthuswamy, P. R. Kharel, G. Lawes, S. L. Brock, *ACS Nano* **2009**, *3*, 2383.
[14] a) A. E. Henkes, Y. Vasquez, R. E. Schaak, *J. Am. Chem. Soc.* **2007**, *129*, 1896; b) A. E. Henkes, R. E. Schaak, *Chem. Mater.* **2007**, *19*, 4234; c) A. E. Henkes, R. E. Schaak, *Inorg. Chem.* **2008**, *47*, 671; d) Y. W. Jun, J. S. Choi, J. Cheon, *Angew. Chem.* **2006**, *118*, 3492; *Angew. Chem. Int. Ed.* **2006**, *45*, 3414.
[15] a) Y. Li, M. A. Malik, P. O'Brien, *J. Am. Chem. Soc.* **2005**, *127*, 16020; b) A. T. Kelly, I. Rusakova, T. Ould-Ely, C. Hofmann, A. Lüttge, K. H. Whitmire, *Nano Lett.* **2007**, *7*, 2920.
[16] a) Q. Yang, K. B. Tang, Q. R. Li, H. Yin, C. R. Wang, Y. T. Qian, *Nanotechnology* **2004**, *15*, 918; b) J. L. Wang, Q. Yang, *Dalton Trans.* **2008**, 6060; c) J. L. Wang, Q. Yang, *Chem. Lett.* **2008**, *37*, 306; d) J. L. Wang, Q. Yang, Z. D. Zhang, T. W. Li, S. Y. Zhang, *Dalton Trans.* **2010**, *39*, 227.
[17] A. P. Grosvenor, S. D. Wik, R. G. Cavell, A. Mar, *Inorg. Chem.* **2005**, *44*, 8988.
[18] D. L. Leslie-Pelecky, R. D. Rieke, *Chem. Mater.* **1996**, *8*, 1770.
[19] a) R. L. Wells, W. L. Gladfelter, *J. Cluster Sci.* **1997**, *8*, 217; b) W. E. Buhro, *Polyhedron* **1994**, *13*, 1131; c) J. M. Nedeljković, O. I. Mićić, S. P. Ahrenkiel, A. Miedaner, A. J. Nozik, *J. Am. Chem. Soc.* **2004**, *126*, 2632; d) F. D. Wang, W. E. Buhro, *J. Am. Chem. Soc.* **2007**, *129*, 14381; e) S. Xu, S. Kumar, T. Nann, *J. Am. Chem. Soc.* **2006**, *128*, 1054.
[20] a) P. E. Fanta, *Chem. Rev.* **1946**, *38*, 139; b) A. Klapars, J. C. Antilla, X. H. Huang, S. L. Buchwald, *J. Am. Chem. Soc.* **2001**, *123*, 7727; c) J. Hassan, M. Sevignon, C. Gozzi, E. Schulz, M. Lemaire, *Chem. Rev.* **2002**, *102*, 1359.
[21] More information about the chemical properties of biphenyl can be found at http://www.npi.gov.au/substances/biphenyl/index.html.
[22] a) G. E. Davico, V. M. Bierbaum, C. H. DePuy, G. B. Ellison, R. R. Squires, *J. Am. Chem. Soc.* **1995**, *117*, 2590; b) K. K. Thoen, H. I. Kenttamaa, *J. Am. Chem. Soc.* **1997**, *119*, 3832.
[23] a) J. K. Kochi, *Free Radicals, Vol. 2, Free Radical Chain Reactions: Structure and Energetics, Free Radicals with Heteroatoms*, Wiley, New York, **1973**; b) R. A. Abramovitch, *Reactive Intermediates*, Plenum Press, New York, **1983**; c) D. I. Davies, M. J. Parrott, *Free Radicals in Organic Synthesis*, Springer, New York, **1978**.

Received: August 2, 2009
Published online: May 20, 2010

